like the incommensurate phase of $Pr_{1/2}Ca_{1/2}MnO_3$, where strong ferromagnetic fluctuations have been measured[14,26], rather than the long-range magnetic order we would predict. Second, in order to keep the calculations tractable, the phase transitions at T_C and T_{CO} have been forced to be continuous. This explains why the re-entrant magnetism above T_L shown in Fig. 2 appears only when $T_C > T_{CO}$. If this theory were generalized to include discontinuous phase transitions, this condition would relax. Another consequence of assuming continuous-phase transitions is that phase separation cannot be predicted. In real systems, phase separation is possible because strain[3,9], or disorder[8], can make more-or-less localized phases dominate within a given region. Orbital ordering is described by a vector order parameter, and thus our simple model cannot address the complexity of different orbitally ordered phases that have been proposed[12].

The Ginzburg–Landau phenomenology we propose is capable of systematizing some puzzling data for manganites near $x = 1/2$, but of course the propensity for mixed and homogeneous phases is driven by the underlying physical parameters that make the energetic cost of spatial fluctuations low. This 'electronic softness' means that as well as spatially disordered 'phase separation', we find new ordered phases which are long-period arrangements of the two competing orders. Indeed, it may be that this potential for textured electronic phases is a hallmark of electronic oxides near the Mott transition[29], seen perhaps in the coexistence of density waves and superconductivity in the copper oxides[30]. □

Received 29 July; accepted 17 December 2004; doi:10.1038/nature03300.

1. Tokura, Y. (ed.) *Colossal Magnetoresistance Oxides* (Gordon and Breach, New York, 2000).
2. Mathur, N. D. & Littlewood, P. B. Mesoscopic textures in manganites. *Phys. Today* **56,** 25–30 (2003).
3. Mathur, N. D. & Littlewood, P. B. The self-organised phases of manganites. *Sol. Stat. Commun.* **119,** 271–280 (2001).
4. Dagotto, E. *Nanoscale Phase Separation and Colossal Magnetoresistance* (Springer Series in Solid State Sciences Vol. 136, Springer, 2002).
5. Uehara, M., Mori, S., Chen, C. H. & Cheong, S.-W. Percolative phase separation underlies colossal magnetoresistance in mixed-valence manganites. *Nature* **399,** 560–563 (1999).
6. Loudon, J. C., Mathur, N. D. & Midgley, P. A. Charge-ordered ferromagnetic phase in $La_{0.5}Ca_{0.5}MnO_3$. *Nature* **420,** 797–800 (2002).
7. Chen, C. H. & Cheong, S.-W. Commensurate to incommensurate charge ordering and its real-space images in $La_{0.5}Ca_{0.5}MnO_3$. *Phys. Rev. Lett.* **76,** 4042–4045 (1996).
8. Burgy, J., Moreo, A. & Dagotto, E. Relevance of cooperative lattice effects and correlated disorder in phase separation theories for CMR manganites. *Phys. Rev. Lett.* **92,** 097202 (2004).
9. Ahn, K. H., Lookman, T. & Bishop, A. R. Strain-induced metal–insulator phase coexistence in perovskite manganites. *Nature* **428,** 401–404 (2004).
10. Goodenough, J. Theory of the role of covalence in the perovskite-type manganites [La, M(II)]MnO_3. *Phys. Rev* **100,** 564–573 (1955).
11. Herrero-Martín, J., García, J., Subías, G., Blasco, J. & Sánchez, M. C. Structural origin of dipole x-ray resonant scattering in the low-temperature phase of $Nd_{0.5}Sr_{0.5}MnO_3$. *Phys. Rev. B* **70,** 024408 (2004).
12. Brey, L. Continuous charge modulated diagonal phase in manganites. *Phys. Rev. Lett.* **92,** 127202 (2004).
13. Coey, M. Charge ordering in oxides. *Nature* **430,** 155–156 (2004).
14. Kajimoto, R., Yoshizawa, H., Tomioka, Y. & Tokura, Y. Commensurate-incommensurate transition in the melting process of orbital ordering in $Pr_{0.5}Ca_{0.5}MnO_3$: A neutron diffraction study. *Phys. Rev. B* **63,** 212407 (2001).
15. Zimmermann, M. v. *et al.* X-ray resonant scattering studies of orbital and charge ordering in $Pr_{1-x}Ca_xMnO_3$. *Phys. Rev. B* **64,** 195133 (2001).
16. Larochelle, S. *et al.* Nature of e_g electron order in $La_{1-x}Sr_{1+x}MnO_4$. *Phys. Rev. Lett.* **87,** 095502 (2001).
17. Jirak, Z., Krupicka, S., Simsa, Z., Dlouham, M. & Vratislav, S. Neutron diffraction study of $Pr_{1-x}Ca_xMnO_3$ perovskites. *J. Magn. Magn. Mater.* **53,** 153–166 (1985).
18. Chen, C. H., Cheong, S.-W. & Hwang, H. Y. Charge ordered stripes in $La_{1-x}Ca_xMnO_3$. *J. Appl. Phys.* **81,** 4326–4330 (1997).
19. Chen, C. H., Mori, S. & Cheong, S.-W. Anomalous melting transition of the charge ordered state in manganites. *Phys. Rev. Lett.* **83,** 4792–4795 (1999).
20. Loudon, J. C. *et al.* Weak charge-lattice coupling requires reinterpretation of stripes of charge order in (La, Ca)MnO_3. Preprint at ⟨http://www.arXiv.org/cond-mat/0308581⟩ (2003).
21. Schiffer, P., Ramirez, A. P., Bao, W. & Cheong, S.-W. Low temperature magnetoresistance and the magnetic phase diagram of $La_{1-x}Ca_xMnO_3$. *Phys. Rev. Lett.* **75,** 3336–3339 (1995).
22. Yoshizawa, H., Kawano, H., Tomioka, Y. & Tokura, Y. Neutron diffraction study of the magnetic-field-induced metal-insulator transition in $Pr_{0.7}Ca_{0.3}MnO_3$. *Phys. Rev. B* **52,** R13145–R13148 (1995).
23. Tolèdano, J. C. & Tolèdano, P. *The Landau Theory of Phase Transitions* Ch. 5 (World Scientific, Singapore, 1987).
24. Murakami, S. & Nagaosa, N. Colossal magnetoresistance in manganites as multicritical phenomena. *Phys. Rev. Lett.* **90,** 197201 (2003).
25. Yamada, Y. & Takakura, T. Incommensurate orbital order and two-phase coexistence in doped manganites at metal-insulator phase boundary. *J. Phys. Soc. Jpn* **71,** 2480–2484 (2002).
26. Kajimoto, R. *et al.* Anomalous ferromagnetic spin fluctuations in an antiferromagnetic insulator $Pr_{1-x}Ca_xMnO_3$. *Phys. Rev. B* **58,** R11837–R11840 (1998).
27. Mathur, N. D. *et al.* Resistance of a domain wall in $La_{0.7}Ca_{0.3}MnO_3$. *J. Appl. Phys.* **86,** 6287–6290 (1999).
28. Rzchowski, M. S. & Joynt, R. Electronic inhomogeneity at magnetic domain walls in strongly-correlated systems. *Europhys. Lett.* **67,** 287–293 (2004).
29. Kivelson, S. A., Fradkin, E. & Emery, V. J. Electronic liquid-crystal phases of a doped Mott insulator. *Nature* **393,** 550–553 (1998).
30. McElroy, K. *et al.* Homogenous nodal superconductivity coexisting with inhomogeneous charge order in strongly underdoped Bi-2212. Preprint at ⟨http://www.arXiv.org/cond-mat/0404005⟩ (2004).

Supplementary Information accompanies the paper on **www.nature.com/nature**.

Acknowledgements We thank L. Brey and N. Mathur for discussions. P.B.L. thanks the National High Magnetic Field Laboratory of the Los Alamos National Laboratory for hospitality. M.J.C. acknowledges Churchill College, University of Cambridge, for the award of a JRF. This work was supported by the EPSRC and through the EPSRC Magnetic Oxide Network.

Competing interests statement The authors declare that they have no competing financial interests.

Correspondence and requests for materials should be addressed to G.C.M. (gcm24@cam.ac.uk).

Synthesis of the H-cluster framework of iron-only hydrogenase

Cédric Tard[1], Xiaoming Liu[1], Saad K. Ibrahim[1], Maurizio Bruschi[3], Luca De Gioia[3], Siân C. Davies[1], Xin Yang[4], Lai-Sheng Wang[4], Gary Sawers[2] & Christopher J. Pickett[1]

[1]*Department of Biological Chemistry,* [2]*Department of Molecular Microbiology, John Innes Centre, Norwich NR4 7UH, UK*
[3]*Department of Biotechnology and Biosciences, University of Milano-Bicocca, Piazza della Scienza 2, 20126-Milan, Italy*
[4]*Department of Physics, Washington State University, 2710 University Drive, Richland, and WR Wiley Environmental Science Laboratory and Chemical Sciences Division, Pacific Northwest National Laboratory, PO Box 999, MS K8-88, Richland, Washington 99352, USA*

The metal-sulphur active sites of hydrogenases catalyse hydrogen evolution or uptake at rapid rates. Understanding the structure and function of these active sites—through mechanistic studies of hydrogenases[1–4], synthetic assemblies[5–12] and *in silico* models[13–15]—will help guide the design of new materials for hydrogen production or uptake[16]. Here we report the assembly of the iron-sulphur framework of the active site of iron-only hydrogenase (the H-cluster), and show that it functions as an electrocatalyst for proton reduction. Through linking of a di-iron subsite to a {4Fe4S} cluster, we achieve the first synthesis of a metallosulphur cluster core involved in small-molecule catalysis. In addition to advancing our understanding of the natural biological system, the availability of an active, free-standing analogue of the H-cluster may enable us to develop useful electrocatalytic materials for application in, for example, reversible hydrogen fuel cells. (Platinum is currently the preferred electrocatalyst for such applications, but is expensive, limited in availability and, in the long term, unsustainable[17].)

The crystallographic characterization of Fe-only hydrogenases[1,2] has revealed a striking resemblance of the di-iron subsite of the H-cluster to known $[Fe_2(\mu\text{-}SR)_2(CO)_6]$ (R = organic group) complexes. This type of assembly, first discovered[18] more than 70 years ago, opened the way for the synthesis of {2Fe2S}- and {2Fe3S}-complexes with key structural and/or spectroscopic features of this biologically unprecedented—low-valent, carbon monoxide- and cyanide-coordinated—di-iron unit (Fig. 1). A major challenge is now to build a free-standing analogue of the entire H-cluster, as this offers the prospects of understanding the interplay of the conjoined di-iron and cubane units that form the enzymic catalytic machinery

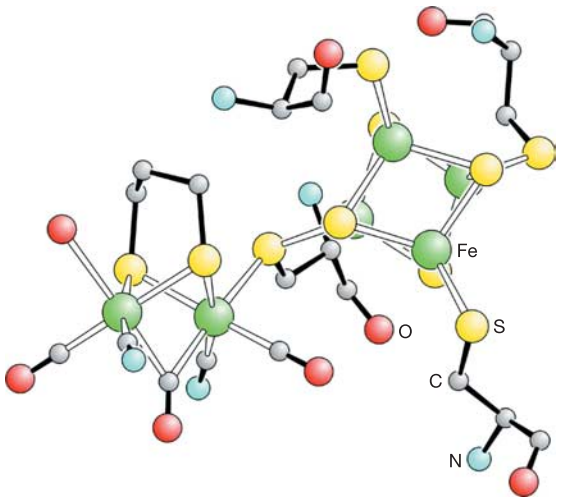

Figure 1 Composite structure of the H-cluster. This was constructed from the crystal structures of Fe-only hydrogenase isolated from *Desulfovibrio desulfuricans* (Protein Data Bank Code 1HFE)[2] and *Clostridium pasteurianum* (Protein Data Bank Code 1FEH)[1], and FTIR data from *Desulfovibrio vulgaris*. The apical group on the sub-site ligand may possibly be an NH, but this remains crystallographically and analytically unresolved.

and of the development of new catalytic materials.

The dithiolate ligand **A**, which possesses an appended thioester group, was synthesized as outlined in Fig. 2. **A** reacts with $Fe_3(CO)_{12}$ to give the thioester activated di-iron subsite analogue, **B**. Unlike dithiolate thioether ligands with the same tripodal carbon backbone[19], the thioester sulphur does not displace CO and coordinate to an Fe atom of the di-iron unit, as shown in the X-ray crystallographic structure (Supplementary Fig. 1). Undoubtedly this is because the electron-withdrawing acyl group lowers the nucleophilicity of the S atom to which it is attached.

The cubane cluster $[Fe_4S_4(L)(SEt)]^{2-}$ (L = 1,3,5-tris (4,6-dimethyl-3-mercaptophenylthio)-2,4,6-tris (*p*-tolyl-thio)benzene), denoted **C**, which has three of the cubane iron atoms blocked by the chelating ligand, was synthesized by an established procedure[20]. **C** reacts cleanly with one equivalent of **B** over a 12 h period at room temperature to give, after work-up, analytically pure $[Fe_4S_4(L)_3\{Fe_2(CH_3C(CH_2S)_3)(CO)_5\}][NBu_4]_2$, **D** (Fig. 2). Negative ion electrospray mass spectrometry (ESMS; MeCN) on **D** showed peaks centred at mass/charge (m/z) = 856.9 (100%) for the dianion and at m/z = 1,957.1 (10%) for $\{[Fe_4S_4(L)_3\{Fe_2(CH_3C(CH_2S)_3)(CO)_5\}]^{2-}[NBu_4]^+\}$, with respective isotopic distribution patterns consistent with doubly and singly charged species. Fourier transform infrared (FTIR) ν(CO) bands for **D** at 2,035(medium, m), 1,970(strong, s) and 1,912(weak, w) cm^{-1} are very similar to those of $[Fe_2(CH_3C(CH_2S)_2(CH_2SCH_3))(CO)_5]$ (2,049(m), 1,983(s) and 1,927(w) cm^{-1}) in which the thioether ligand is known to be coordinated to one Fe atom[19]. Thus the reaction between **B** and **C** proceeds beyond elimination of MeCOSEt—carbon monoxide is lost from the proximal Fe atom of the di-iron unit, and results in the formation of a $\{Fe_{cubane}(\mu-SR)Fe_{subsite}\}$ linkage as found in the H-cluster (Fig. 3). This is supported by the solid state Mössbauer spectrum of **D** at 80 K, which exhibits four overlapping quadrupole split doublets with isomer shift (i.s.) and quadrupole splitting (q.s.) parameters (in $mm\,s^{-1}$) consistent with four differentiated iron sites; two associated with the site-differentiated cubane (i.s. = 0.47, q.s. = 1.14; i.s. = 0.45, q.s. = 0.87) and two with the di-iron subsite (i.s. = 0.04, q.s. = 1.00 (Fe distal to cubane); i.s. = 0.04, q.s. = 0.50 (Fe proximal to cubane))[19].

Full geometry optimization of an *in silico* model of **D**, $[Fe_4S_4(SCH_3)_3\{Fe_2(CH_3C(CH_2S)_3)(CO)_5\}]^{2-}$, was carried out in the density functional theory (DFT) framework using the BP86 pure functional[21,22] and an all-electron valence triple-ζ basis set with polarization functions on all atoms (TZVP)[23]. This resulted in a structure fully consistent with that proposed on the basis of experimental data for **D** (Fig. 3). In particular, one of the thiolate groups bridges almost symmetrically the {4Fe4S} and the {2Fe2S} units, with an Fe–Fe distance (2.6 Å) in the binuclear cluster that is indicative of a metal–metal bond. Analysis of the electronic properties of the *in silico* structure reveals that the redox state of the binuclear moiety can be described as Fe(I)Fe(I).

The $\{Fe_{cubane}(\mu\text{-}SR)Fe_{subsite}\}$ linkage provides substantial electronic communication between the di-iron centre and the {4Fe4S} cubane centre, as is evident from the following spectroscopic and electrochemical measurements. Formally replacing the Me of the thioether ligand in $[Fe_2(CH_3C(CH_2S)_2(CH_2SCH_3))(CO)_5]$ by the cubane dianion shifts all the ν(CO) frequencies of the appended subsite by ~15 cm^{-1} to lower values: the $\{Fe_4S_4(L)\}^{2-}$-core is a 'better' donor group than is methyl. The inductive influence of the cubane in lowering ν(CO) is reciprocated in the shift of the redox

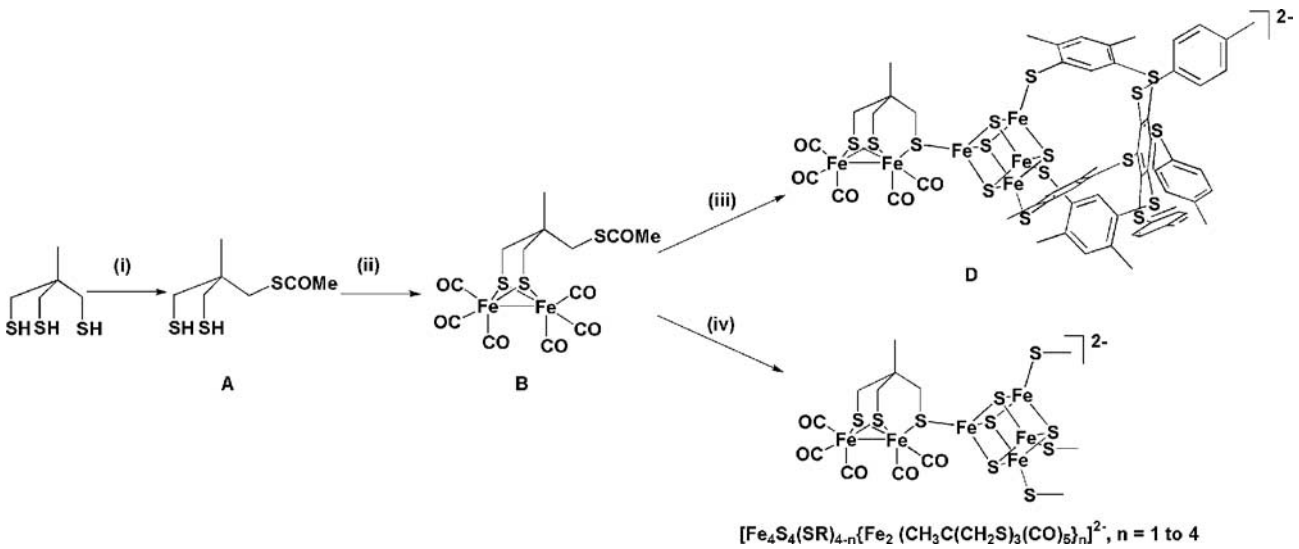

Figure 2 Synthetic pathways for assembly of the H-cluster model and related subsite-cluster materials. Reaction steps are as follows: (i) acetic anhydride, $NaHCO_3$, diethyl ether, (ii) $Fe_3(CO)_{12}$, toluene, (iii) **C**, MeCN, (iv) $[Fe_4S_4(SEt)_4][NBu_4]_2$, MeCN.

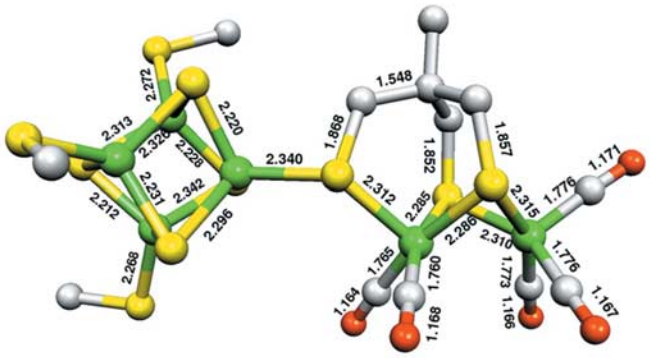

Figure 3 Structure of $[Fe_4S_4(SCH_3)_3\{Fe_2(CH_3C(CH_2S)_3)(CO)_5\}]^{2-}$, derived from DFT calculations. Numbers show bond lengths in Å.

potential for the reduction of the cubane core to more positive potentials. The primary reversible one-electron reduction of **D** (0.1 M $[NBu_4][BF_4]$-MeCN, cyclic voltammetry, sweep rate 100 mV s^{-1}) occurs at $E_{1/2} = -0.86$ V versus (Ag/AgCl, CH_2Cl_2, 0.45 M $[NBu_4][BF_4]$, 0.05 M $[NBu_4]Cl$); that for the parent cluster $[Fe_4S_4(L)(SEt)]^{2-}$ is at $E_{1/2} = -0.98$ V under identical conditions. The $\Delta E_{1/2}$ for the formal replacement of EtS by $\{Fe_2(CH_3C(CH_2S)_3)(CO)_5\}$ of +120 mV shows that the energy of the cubane lowest unoccupied molecular orbital (LUMO) is substantially lowered.

Gas-phase photoelectron spectroscopy (PES)[24,25] of isolated $[Fe_4S_4(SEt)_3\{Fe_2(CH_3C(CH_2S)_3)(CO)_5\}]^{2-}$ is concordant with this. The PES of this anion at an excitation wavelength of 355 nm revealed two low-binding-energy spectral features that are very similar to the first two bands of $[Fe_4S_4(SEt)_4]^{2-}$ but shifted by about 0.6 eV to higher energy (adiabatic electron detachment energy increases from 0.29 to 0.89 eV (ref. 26); Supplementary Fig. 2). Thus on replacing EtS by the subsite unit the highest-energy orbitals remain localized on the cubane core but are substantially stabilized. At 266 and 193 nm, higher-energy spectral features associated with the attached subsite are also observed that are absent in the parent dianion, $[Fe_4S_4(SEt)_4]^{2-}$.

Complete substitution of the {4Fe4S}-core by di-iron units is possible (Fig. 2, step (iv)). The reaction of $[Fe_4S_4(SEt)_4][NBu_4]_2$ (MeCN, room temperature, 12 h) with an excess of **B** followed by work-up and ESMS shows formation of a dianion with *m*/*z* centred at 1,009.6 (100%) and an isotopic pattern corresponding to the dianion $[Fe_4S_4\{Fe_2(CH_3C(CH_2S)_3)(CO)_5\}_4]^{2-}$, **E**. Cyclic voltammetry of **E** (vitreous carbon electrode, 100 mV s^{-1}, room temperature, 0.1 M $[NBu_4][BF_4]$-CH_2Cl_2) shows a primary reversible one-electron reduction couple at −0.65 V versus (Ag/AgCl, CH_2Cl_2, 0.45 M $[NBu_4][BF_4]$, 0.05 M $[NBu_4]Cl$) corresponding to the reduction of the $\{4Fe4S\}^{2+}$ core, and a multi-electron reduction at −1.58 V which encompasses the irreversible reduction of the subsite units. The primary reversible reduction of $[Fe_4S_4(SEt)_4]^{2-}$ occurs at −1.15 V under the same conditions, attesting to the strong electron-withdrawing properties of the μ-S ligated di-iron subsites. The ΔE of +500 mV for replacement of the four EtS ligands by four subsite ligands (that is, an average of 125 mV per substitution) fits very well with the 120 mV shift observed on replacing the single EtS with the di-iron subsite to give **D**.

Beyond inductive effects transmitted through the $\{2Fe2S\}(\mu\text{-}SCH_2R)\{4Fe4S\}$ framework, there is evidence for an interplay of redox states that transcends the behaviour of the isolated component di-iron and the cubane centre. Repetitive cyclic voltammetry of **D** over 10 cycles shows the build-up of a reversible system at −0.96 V versus (Ag/AgCl, CH_2Cl_2, 0.45 M $[NBu_4][BF_4]$, 0.05 M $[NBu_4]Cl$) (Fig. 4a and Supplementary Fig. 3 (process II)). The voltammogram can be reasonably simulated by a mechanism that involves intramolecular electron transfer between the reduced cluster and subsite in concert with reversible opening of the μ-SCH_2 bridge. This leaves the cubane linked to the subsite by an alkylthiolate in a $\{4Fe4S\}^{2+}$ state and therefore susceptible to further reduction. This would be expected to take place at a potential close to that observed for the alkylthiolate ligated $[Fe_4S_4(L)(SEt)]^{2-}$, as is observed (Supplementary Fig. 4 and Supplementary Text).

Studies[11,27] have shown that simple subsite models are capable of electrocatalysing proton reduction and H/D exchange reactions, albeit at low reduction potentials[12,28]. Figure 4b shows that the H-cluster analogue **D** electrocatalyses proton reduction at a diffusion-controlled rate. The current–potential curve for the reduction of protons in the presence of the catalyst (E_p=−1.13 V) is displaced by ~200 mV positive from that measured in the absence of the catalyst ($E_p = -1.33$ V versus (Ag/AgCl, CH_2Cl_2, 0.45 M $[NBu_4][BF_4]$, 0.05 M $[NBu_4]Cl$)).

The μ-S cysteinyl bridge identified in the enzyme structures[1,2] must provide substantial electronic communication between the subsite and the {4Fe4S}-cubane, because we have shown for **D** that these units do not behave as insulated redox entities. The Mössbauer parameters for **D** corrected for the second order Doppler effect to 4.2 K (site differentiated cubane: i.s. = 0.50, 0.48, q.s. = 0.87, 1.14; di-iron subsite: i.s. = 0.07,0.07 q.s. = 0.50, 1.00 mm s^{-1}) are similar to those attributed to these components in the reduced state of *Clostridium pasteurianum* hydrogenase II (site differentiated

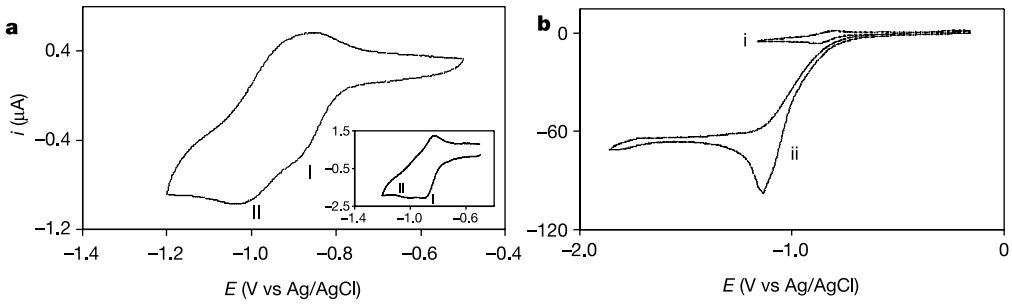

Figure 4 The electrochemical behaviour of the synthetic H-cluster model. **a**, Cyclic voltammogram of **D** (0.1 M $[NBu_4][BF_4]$-MeCN, 30 mV s^{-1}, vitreous carbon), showing interconverting redox processes I and II. $E_{1/2}$ for II occurs at a potential close to that for **C**, indicative of the rearrangement of the μ-S bonded subsite to the terminal alkylthiolate. Inset, first-scan response at the faster scan rate of 0.1 V s^{-1} but otherwise under the same conditions; note suppression of the interconversion. **b**, Cyclic voltammogram of **D** (1.5 mM), showing the electrocatalytic response in the absence (trace i) and in the presence (trace ii) of 4,6-dimethyl pyridinium cation as a source of protons (15 mM) at a normalized scan rate of 0.1 V s^{-1}. The peak current for proton reduction in the absence of the catalyst is within 5% of that in its presence, but is shifted about 200 mV to a more negative potential.

cubane: i.s. = 0.47, 0.47, q.s. = 0.85, 1.35; di-iron subsite: i.s. = 0.08, q.s. = 0.87 mm s^{-1}) measured at 4.2 K. This is concordant with the generally accepted re-assignment of the electronic structure of the six-iron core of the reduced biological cluster as $[\{Fe(I).Fe(I)\}_{subsite}\text{-}\{4Fe4S\}^{2+}_{cubane}]$[29], the established redox configuration of our synthetic cluster. In the synthetic system, we have seen that the reduction of the cubane unit by one electron to the $\{4Fe4S\}^{+}$ level is easier than is reduction of the $\{Fe(I).Fe(I)\}_{subsite}$, which is coordinatively saturated with a closed-shell (36-electron) configuration. A corresponding state of the H-cluster, in which the cubane unit is reduced to the $\{4Fe4S\}^{+}$ level, has yet to be detected, although neighbouring {4Fe4S} relay centres in *C. pasteurianum* hydrogenase II can be reduced to this level[29]. This raises the question as to whether the $\{4Fe4S\}^{+}$ level of the H-cluster is physiologically accessed during turnover. A vacant or (weakly) water-coordinated site has been identified crystallographically in the enzyme at the distal iron atom in the resting state of the enzyme. It is possible that protonation at this site lowers the energy of the Fe(I)·Fe(I) subsite unit sufficiently to enable its reduction by the anchored cubane operating at the $\{4Fe4S\}^{2+}$ level. That **D** is capable of electrocatalysing proton reduction may be similarly linked to the formation of a vacant site, in this case by the opening of the μ-S bridge on reduction.

The artificial H-clusters reported here should enhance our understanding of the intimate chemistry of the natural process, and lead to systems with low overpotentials for hydrogen uptake/evolution[11,28]. Given that redox-active $\{4Fe4S\}^{2+}$-centres can be incorporated at high concentration into cysteine functionalized electropolymers[30], we can envisage their modification, using the chemistry we have described, thereby providing a route to advanced electrode materials. □

Received 14 October; accepted 14 December 2004; doi:10.1038/nature03298.

1. Peters, J. W., Lanzilotta, W. N., Lemon, B. J. & Seefeldt, L. C. X-ray crystal structure of the Fe-only hydrogenase (Cpl) from *Clostridium pasteurianum* to 1.8 angstrom resolution. *Science* **282,** 1853–1858 (1998).
2. Nicolet, Y., Piras, C., Legrand, P., Hatchikian, C. E. & Fontecilla-Camps, J. C. *Desulfovibrio desulfuricans* iron hydrogenase: the structure shows unusual coordination to an active site Fe binuclear center. *Struct. Fold. Des.* **7,** 13–23 (1999).
3. Nicolet, Y., Lemon, B. J., Fontecilla-Camps, J. C. & Peters, J. W. A novel FeS cluster in Fe-only hydrogenases. *Trends Biochem. Sci.* **25,** 138–143 (2000).
4. Armstrong, F. A. Hydrogenases: active site puzzles and progress. *Curr. Opin. Chem. Biol.* **8,** 133–140 (2004).
5. Evans, D. J. & Pickett, C. J. Chemistry and the hydrogenases. *Chem. Soc. Rev.* **32,** 268–275 (2003).
6. Lyon, E. J., Georgakaki, I. P., Reibenspies, J. H. & Darensbourg, M. Y. Carbon monoxide and cyanide ligands in a classical organometallic complex model for Fe-only hydrogenase. *Angew. Chem. Int. Edn* **38,** 3178–3180 (1999).
7. Schmidt, M., Contakes, S. M. & Rauchfuss, T. B. First generation analogues of the binuclear site in the Fe-only hydrogenases: $Fe_2(\mu\text{-}SR)_2(CO)_4(CN)_2^{2-}$. *J. Am. Chem. Soc.* **121,** 9736–9737 (1999).
8. Le Cloirec, A. *et al.* A di-iron dithiolate possessing structural elements of the carbonyl/cyanide sub-site of the H-centre of Fe-only hydrogenase. *Chem. Commun.* 2285–2286 (1999).
9. Razavet, M. *et al.* Transient FTIR spectroelectrochemical and stopped-flow detection of a mixed valence {Fe(I)-Fe(II)} bridging carbonyl intermediate with structural elements and spectroscopic characteristics of the di-iron sub-site of all-iron hydrogenase. *Chem. Commun.* 700–701 (2002).
10. George, S. J., Cui, Z., Razavet, M. & Pickett, C. J. The di-iron subsite of all-iron hydrogenase: Mechanism of cyanation of a synthetic {2Fe3S} – carbonyl assembly. *Chem. Eur. J.* **8,** 4037–4046 (2002).
11. Gloaguen, F., Lawrence, J. D., Rauchfuss, T. B., Benard, M. & Rohmer, M. M. Bimetallic carbonyl thiolates as functional models for Fe-only hydrogenases. *Inorg. Chem.* **41,** 6573–6582 (2002).
12. Ott, S., Kritikos, M., Akermark, B., Sun, L. C. & Lomoth, R. A biomimetic pathway for hydrogen evolution from a model of the iron hydrogenase active site. *Angew. Chem. Int. Edn* **43,** 1006–1009 (2004).
13. Cao, Z. X. & Hall, M. B. Modeling the active sites in metalloenzymes. 3. Density functional calculations on models for Fe-hydrogenase: Structures and vibrational frequencies of the observed redox forms and the reaction mechanism at the diiron active center. *J. Am. Chem. Soc.* **123,** 3734–3742 (2001).
14. Liu, Z. P. & Hu, P. A density functional theory study on the active center of Fe-only hydrogenase: Characterization and electronic structure of the redox states. *J. Am. Chem. Soc.* **124,** 5175–5182 (2002).
15. Bruschi, M., Fantucci, P. & De Gioia, L. Density functional theory investigation of the active site of Fe-hydrogenases. Systematic study of the effects of redox state and ligands hardness on structural and electronic properties of complexes related to the $[2Fe]_H$ subcluster. *Inorg. Chem.* **43,** 3733–3741 (2004).
16. *Basic Research Needs for the Hydrogen Economy* (Report of the Basic Energy Sciences Workshop on Hydrogen Production, Storage, and Use, 13–15 May 2003, Office of Science, US Department of Energy); available at ⟨http://www.eere.energy.gov/hydrogenandfuelcells/pdfs/bes_project.pdf⟩.
17. *Platinum and Hydrogen for Fuel Cell Vehicles* (UK Department for Transport, September 2003); available at ⟨http://www.dft.gov.uk/stellent/groups/dft_roads/documents/page/dft_roads_024056.hcsp⟩.
18. Reihlen, H., Gruhl, A. & Hessling, G. Über den photochemischen und oxydativen Abbau von Carbonylen. *Liebigs Ann. Chem.* **472,** 268–287 (1929).
19. Razavet, M. *et al.* All-iron hydrogenase: synthesis, structure and properties of {2Fe3S}-assemblies related to the di-iron sub-site of the H-cluster. *Dalton Trans.* 586–595 (2003).
20. Stack, T. D. P. & Holm, R. H. Subsite-specific functionalization of the $[4Fe\text{-}4S]^{2+}$ analog of iron sulfur protein clusters. *J. Am. Chem. Soc.* **109,** 2546–2547 (1987).
21. Perdew, J. P. Density-functional approximation for the correlation-energy of the inhomogeneous electron-gas. *Phys. Rev. B* **33,** 8822–8824 (1986).
22. Becke, A. D. Density-functional exchange-energy approximation with correct asymptotic-behavior. *Phys. Rev. A.* **38,** 3098–3100 (1988).
23. Schafer, A., Huber, C. & Ahlrichs, R. Fully optimized contracted Gaussian-basis sets of triple zeta valence quality for atoms Li to Kr. *J. Chem. Phys.* **100,** 5829–5835 (1994).
24. Wang, L. S., Ding, C. F., Wang, X. B. & Barlow, S. E. Photodetachment photoelectron spectroscopy of multiply charged anions using electrospray ionization. *Rev. Sci. Instrum.* **70,** 1957–1966 (1999).
25. Yang, X., Razavet, M., Wang, X. B., Pickett, C. J. & Wang, L. S. Probing the electronic structure of the di-iron subsite of Fe-hydrogenase: A photoelectron spectroscopic study of Fe(I)-Fe(I) model complexes. *J. Phys. Chem. A* **107,** 4612–4618 (2003).
26. Wang, X. B. *et al.* Probing the intrinsic electronic structure of the cubane [4Fe4S] cluster: Nature's favorite cluster for electron transfer and storage. *J. Am. Chem. Soc.* **125,** 14072–14081 (2003).
27. Zhao, X. *et al.* Catalysis of H_2/D_2 scrambling and other H/D exchange processes by [Fe]-hydrogenase model complexes. *Inorg. Chem.* **41,** 3917–3928 (2002).
28. Tard, C., Liu, X., Hughes, D. L. & Pickett, C. J. A novel $\{Fe^{I}\text{-}Fe^{II}\text{-}Fe^{II}\text{-}Fe^{I}\}$ iron thiolate carbonyl assembly which electrocatalyses hydrogen evolution. *Chem. Commun.* 133–135 (2005).
29. Popescu, C. V. & Munck, E. Electronic structure of the H cluster in Fe-hydrogenases. *J. Am. Chem. Soc.* **121,** 7877–7884 (1999).
30. Pickett, C. J. & Ryder, K. S. Bioinorganic reaction centers on electrodes — Modified electrodes possessing amino-acid, peptide and ferredoxin-type groups on a poly(pyrrole) backbone. *J. Chem. Soc. Dalton Trans.* 2181–2189 (1994).

Supplementary Information accompanies the paper on **www.nature.com/nature**.

Acknowledgements This work was supported by the BBSRC and the John Innes Foundation. We thank D. J. Evans and J. E. Barclay for Mössbauer spectroscopy and discussions; L. Hill for ESMS; and R. R. Eady and R. A. Dixon for discussions and comments on the manuscript. Research done at Washington State University was supported by NIH and performed at EMSL, a national scientific user facility sponsored by the US DOE's Office of Biological and Environmental Research and located at PNNL, which is operated for DOE by Battelle.

Competing interests statement The authors declare that they have no competing financial interests.

Correspondence and requests for materials should be addressed to C.J.P. (chris.pickett@bbsrc.ac.uk). Crystal structure data for **B** have been deposited at the Cambridge Crystallographic Data Centre, and allocated the deposition number CCDC 256735.

Highly variable Northern Hemisphere temperatures reconstructed from low- and high-resolution proxy data

Anders Moberg[1], Dmitry M. Sonechkin[2], Karin Holmgren[3], Nina M. Datsenko[2] & Wibjörn Karlén[3]

[1]*Department of Meteorology, Stockholm University, SE-106 91 Stockholm, Sweden*
[2]*Dynamical-Stochastical Laboratory, Hydrometeorological Research Centre of Russia, Bolshoy Predtechensky Lane 11/13, Moscow 123 242, Russia*
[3]*Department of Physical Geography and Quaternary Geology, Stockholm University, SE-106 91 Stockholm, Sweden*

A number of reconstructions of millennial-scale climate variability have been carried out in order to understand patterns of natural climate variability, on decade to century timescales, and the role of anthropogenic forcing[1–8]. These reconstructions have mainly used tree-ring data and other data sets of annual to decadal resolution. Lake and ocean sediments have a lower time resolution, but provide climate information at multicentennial timescales that may not be captured by tree-ring data[9,10]. Here we reconstruct Northern Hemisphere temperatures for the past 2,000 years by combining low-resolution proxies with